Acta Geodyn. Geomater., Vol. 20, No. 4 (212), 165–177, 2023
DOI: 10.13168/AGG.2023.0015
journal homepage: https://www.irsm.cas.cz/acta

ORIGINAL PAPER

INTEGRATED ANALYSIS OF GEOPHYSICAL METHODS FOR LANDSLIDE CHARACTERIZATION

Muhammad Taqiuddin ZAKARIA [1)] *, Nordiana Mohd MUZTAZA [2)] * and Nur Azwin ISMAIL [2)]

[1)] *Department of Earth Sciences and Environment, Faculty of Science and Technology, Universiti Kebangsaan Malaysia, 43600 UKM Bangi, Selangor Darul Ehsan, Malaysia*
[2)] *School of Physics, Universiti Sains Malaysia, 11800, USM, Penang, Malaysia*

**Corresponding author's e-mails:* taqiuddin@ukm.edu.my; mmnordiana@usm.my

ARTICLE INFO

Article history:
Received 15 September 2023
Accepted 5 December 2023
Available online 12 December 2023

Keywords:
Resistivity
Seismic refraction
Landslide

ABSTRACT

Landslides are often regarded as secondary hazards, typically triggered by major catastrophic events like storms, floods, volcanic eruptions, and earthquakes. In tropical regions such as Malaysia, the prevalent geohazard phenomenon involves landslides induced by moisture or rainfall. These incidents predominantly occur due to the unique composition of residual soils in the area, resulting from the weathering of bedrock in situ. Major landslides and local slope failures occur when water saturation exceeds a critical limit in certain parts of the slope. The foundation of a dependable stability analysis lies in the geological model of the landslide, which should accurately reflect the actual conditions. To achieve this, a thorough understanding of the landslide phenomenon and access to high-quality datasets are essential. In this study, 2D electrical resistivity imaging and seismic refraction tomography were utilized to identify subsurface characteristics, along with geotechnical data for data corroboration. The study shows a highly weathered zone (ρ< 1200 Ωm; V_p< 1200 m/s) was identified at a depth of less than 5 m. The number of blows (N-values) for standard penetration test (SPT) indicate a low range of 1–15, representing the low stiffness of the soil condition. The N-values show variation in the number of blows with depth, suggesting that the layer may not be competent due to the present heterogeneous material caused by the highly weathered process. The results emphasize the benefits of incorporating both geophysical and geotechnical parameters to define subsurface properties. The study offers insights into how spatial distributions of these parameters can be utilized to minimize uncertainty in ground models.

1. INTRODUCTION

A landslide is the mass movement of materials, such as rock, earth, or debris, down a slope in various shapes and volumes. It causes a significant impact to population, socioeconomic and act as driving force to landscape evolution (Merghadi et al., 2020). Landslides are classified based on types of material being displaced and the mechanism of types movement (falls, topples, slides, flows, spreads) (Hungr et. al., 2014). In certain cases, complex scenario is involved with combination one or more of these type movement. The triggering factors vary between natural forces (precipitation, earthquake, volcanic activity) to human activities (improper land use, overloading, urbanisations) and resulted an imbalance between driving and resisting forces (Christopher et al., 2023). The stability of a slope reflects the balance between driving forces, which cause the movement of earth materials down a slope, and resisting forces, which act against such movement. These forces are influenced by the interplay of various factors, including the type of earth materials, forces acting on the slope, slope angle and topography, weather and vegetation, water, and time. The increasing occurrence of landslide activities, particularly in tropical regions, has heightened the need for comprehensive stability analyses of areas prone to gravitational movements (Rahman and Mapjabil, 2017). Landslides commonly occur during prolonged periods of heavy rainfall, steep slopes, sparse vegetation, and in areas with an abundant source of incoherent fine-grained soils, including colluvium and residual soils especially in tropical and temperate climatic zone where residual soil prevails (Beyene et al., 2023). The foundation of a dependable stability analysis lies in the geological model of the landslide, which should accurately reflect the actual conditions. To achieve this, a thorough understanding of the landslide phenomenon and access to a high-quality dataset are essential (Innocenti et al., 2023). The integration of geophysical, geotechnical, and hydrological datasets provides valuable information to enhance the reliability of deterministic models (Zakaria et al., 2021). The utilisation of geophysical approaches (electrical, seismic, gravity, etc.) is based on delineating the boundaries of geophysical contrasts within the geological medium affected by slide processes, including the failure surface and hydrological properties such as water content within the affected geological medium.

Cite this article as: Zakaria MT, Muztaza NM, Ismail NA: Integrated analysis of geophysical methods for landslide characterization. Acta Geodyn. Geomater., 20, No. 4 (212), 165–177, 2023. DOI: 10.13168/AGG.2023.0015

Understanding the factors that contribute to landslide formation and employing appropriate numerical modeling techniques are crucial for a comprehensive evaluation of landslide mitigations. Investigating the subsurface features of landslides is crucial for obtaining preliminary data for forward modeling and predicting potential failure events (Malet et al., 2005; Rosso et al., 2006). There are various methods available for studying the geometry and stability conditions of landslides, which can be broadly categorized as intrusive (involving boreholes, soil sampling, and laboratory testing) and non-intrusive (geophysical) methods (Kayode et al., 2019; Yordkayhun, 2021; Zaid et al., 2023). While intrusive methods are commonly used, they can be expensive and require accessible areas. The geotechnical approaches provide verifiable information on the mechanical and hydraulic characteristics of landslides, but their limitations lie in providing data only at discrete points within the subsurface (Marcato et al., 2012). Geophysical approaches such as 2D electrical resistivity imaging (ERI) and seismic refraction tomography (SRT) play a major role in landslide characterization. The contrasting physical properties enable the identification of spatial variations in physical parameters, including the extent of the landslide, location of the slip surface, lithological boundaries, distribution of moisture movement within the landslide body, assessment of fractures' formation and growth, as well as understanding water dynamics and the potential for reactivation triggered by rainfall (Whiteley et al., 2019; Pazzi et al., 2019; Zakaria et al., 2022). Nevertheless, owing to the inherent ambiguity in geophysical interpretation and its constrained resolution, it is imperative to complement it with associated geological-engineering information or findings derived from alternative geophysical measurements. In this investigation, the utilization of ERI and SRT methods was directed towards visualizing failure zones and discerning subsurface characteristics correlated with factors that instigate slope failures. Geotechnical data were integrated to substantiate the geophysical interpretation. The ERI method yielded insights into water saturation and landslide geometry, whereas the velocity profile derived from SRT assisted in gauging the stiffness of soil profiles.

2. MATERIAL AND METHODS

2.1. STUDY AREA

The study area is a hillside township situated in Hulu Kelang area, and its vicinity are underlain by granitic beds of Triassic age known as Kuala Lumpur granite, which is a part of the Main Range granite that intruded into folded and regionally metamorphosed clastic and calcareous Palaeozoic rocks (Huat et al., 2012; Ismail et al., 2019). The hilly area is underlain by granite with coarse-grained particles and slightly porphyritic texture. This area also experienced an extreme weathering process which transformed the granite into residual soil (grade V1) and weathered materials (grade V) (Kazmi et al., 2017). The weathered materials were reported as sandy and highly inconsistent with increasing amount of water (Chigira et al., 2011). This area is also surrounded by Hawthornden formation and Kuala Lumpur limestone (Ingham and Bradford, 1960). Another part of the area consists of schist rock known as Schist-Hawthornden of the Ordovician-Silurian age. Quartz vein formation also exists in the granite with NW-E orientation, which is parallel to several sets of Kuala Lumpur fault. This fault, as well as the basin have cut off the regional structure of the region, which is almost northeast. Highly weathered and jointed granitic bedrock underlies the subsoil profile of the area (Ali and Harianto, 2004; Ali and Huat, 2006). The presence of numerous cracks and some minor scale slumping in this area indicate the instability of the slope with angle of 45^{o}-50^{o} (Slope Engineering Branch of the Public Works Department Malaysia, 2008). Moreover, the geomorphology of the study area is mainly controlled by the type of rocks and structures (Ismail et al., 2019). Figure 1 shows the map of study area.

2.2. FIELD PROCEDURE

In this case study, ERI and SRT were designed in lines. In ERI, nine survey lines (BR1-BR9) were aligned parallel to the failed slope (Fig. 1b). *Aktiebolaget Elektrisk Malmletning*-Signal Averaging System (ABEM SAS 4000) was utilised to acquire survey data using an electrode spacing of 5 m. Pole-dipole array was employed in the data protocol acquisition in providing comprehensive data resolutions. Furthermore, in SRT, two survey lines (BS1 and BS2) were designed parallel to the failed slope with a geophone spacing of 5 m. Seismograph ABEM Terraloc Mk8 and a set of geophones of 24 Hz frequency was used to record seismic waves with 5 kg sledgehammer as an impulsive waves source. Table 1 shows the detailed parameters of the survey lines.

In this study, borehole information on SPT-N values was used to validate the geophysical results. Approximately nine boreholes were employed to corroborate the interpretation, as the method provides in-situ site measurements for soil stiffness. Soil stiffness is represented by the increasing number of blows (N-values), with N=50 representing the bedrock of the profile. The N-values reflect changes in the number of blows as depth increases, indicating that the layer may lack competence due to the current heterogeneous material resulting from extensive weathering processes. The locations of the boreholes are shown in Figure 1, and the SPT-N values were correlated in the results.

2.2.1. ERI

The method utilises direct current to investigate the bulk of resistivity distribution of the subsurface. The resistivity value is related to some of the geological parameters, including porosity, fluid

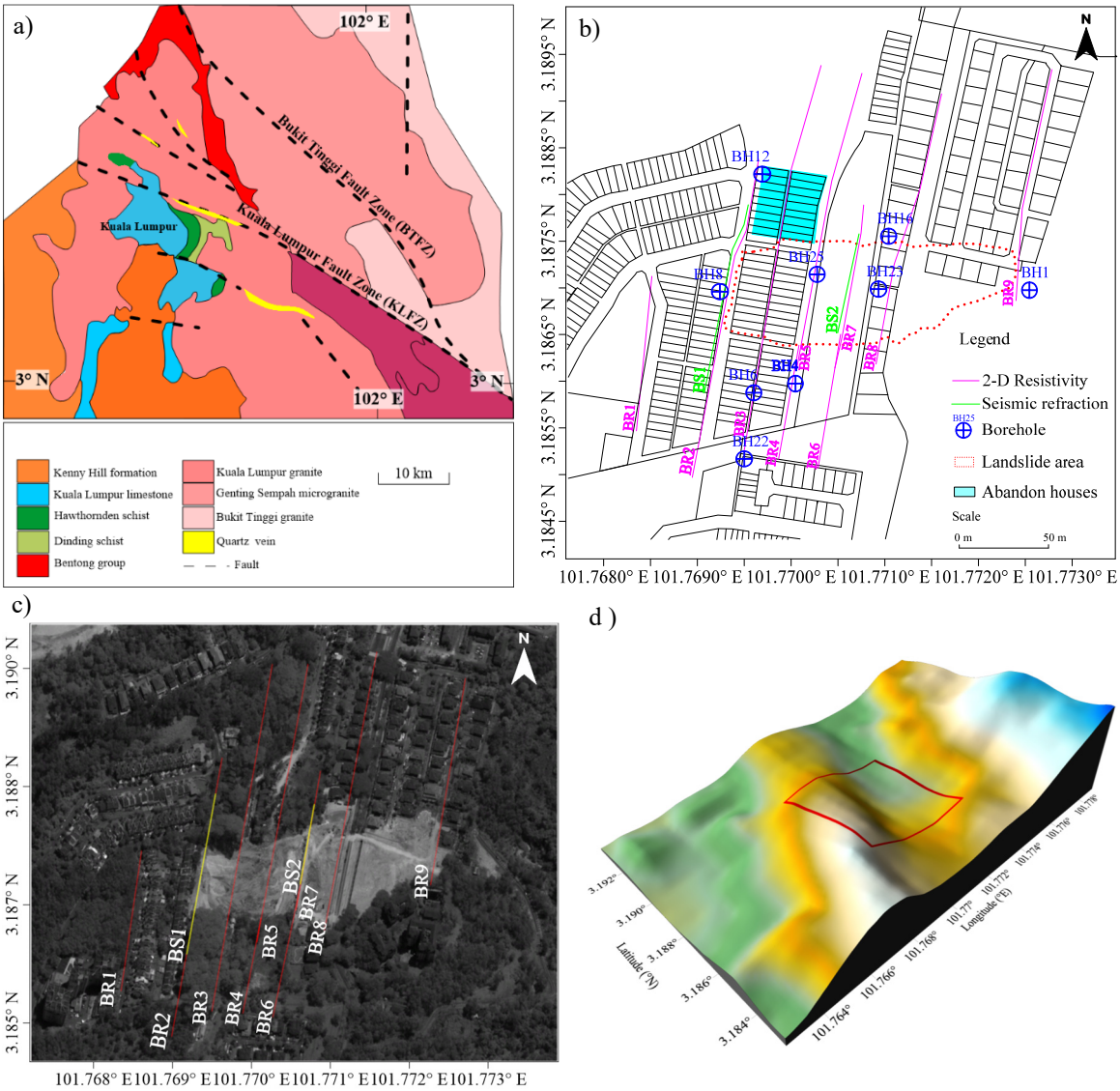

Fig. 1 Study area; a) General geology; b) Simplified survey map of the study area; c) Satellite image from Google Earth Pro; d) The topography model of study area.

Table 1 Survey lines of study area.

Method	No. of line	Total length	Electrodes/geophones spacing	Array
ERI	3 (BR1, BR6, BR7)	200 m	5	Pole-dipole
	4 (BR2, BR3, BR5, BR8)	400 m		
	1 (BR9)	300 m		
	1 (BR4)	165 m		
SRT	1 (BS1)	230 m	5	-
	1 (BS2)	115 m		

content and degree of water saturation in rock. In the resistivity method, electric currents are passed through the surface of the electrodes that are inserted into the ground, thereby resulting in a potential difference. The differences in the patterns of potential difference in the homogenous ground provides information and electrical properties of the subsurface inhomogeneities (Kearey et al., 2013). The current is injected into the ground through two current flowing electrodes: C1 and C2. The potential difference is measured using two potential measurement electrodes, namely P1 and P2. Figure 2 shows the configuration of a four-electrode array.

Moreover, various considerations must be addressed, encompassing the array's responsiveness to alterations in subsurface resistivity, both vertically and horizontally, the depth of investigation, the extent of horizontal data coverage, and signal strength (Loke,

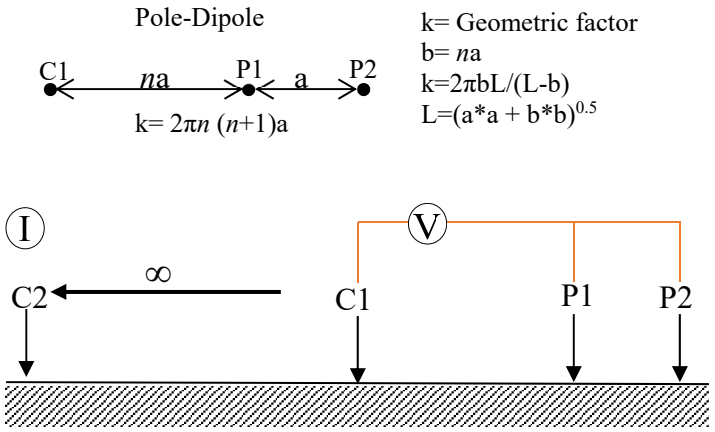

Fig. 2 Anatomy of resistivity electrode configuration and array type.

2015). The pole-dipole array exhibits robust horizontal coverage and a notably higher signal strength. The sensitivity profile demonstrates an increased sensitivity for a larger *n* factor, as this array is more sensitive to vertical structure with good horizontal coverage (Loke, 2015). This array requires a remote electrode, C2, which is placed sufficiently far from survey lines. The effect of C2 electrode is approximately proportional to the square ratio of C1-P1 distance to C2-P1. The remote is placed at a distance of more than five times the largest distance of C1-P1, in order to neglect error by less than 5 % (Loke, 2015). The data processing was conducted using the Res2Dinv software, which employed a mathematical algorithm to generate a 2-D resistivity inversion model. The program utilized an inversion routine based on the smoothness-constrained least-square method (DeGroot-Hedlin et al., 1990; Sasaki, 1992; Loke, 2011). The inversion minimises the error, which determines the degree of discrepancy between calculated apparent resistivity values for the assumed and the input model as the RMS error is adjusted to <20 % for the profiles. The calculated apparent resistivity values of the model block were compared with the measured apparent resistivity values. It was adjusted iteratively until the values of the model achieved a high closeness with the measured apparent resistivity values. Meanwhile, the resistivity contour values were adjusted based on the geological information of the survey area in different colours and resistivity range. Figure 3 shows the overview of ERT data processing.

2.2.2. SRT

The SRT method involves estimating the P-wave velocity (V_p) of the Earth's near-surface material and

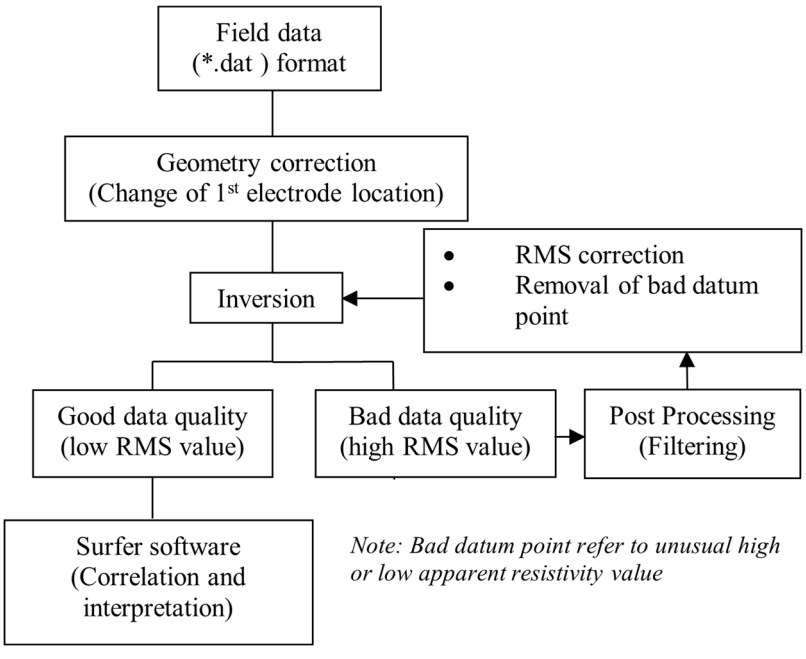

Fig. 3 Flow chart of ERT data processing.

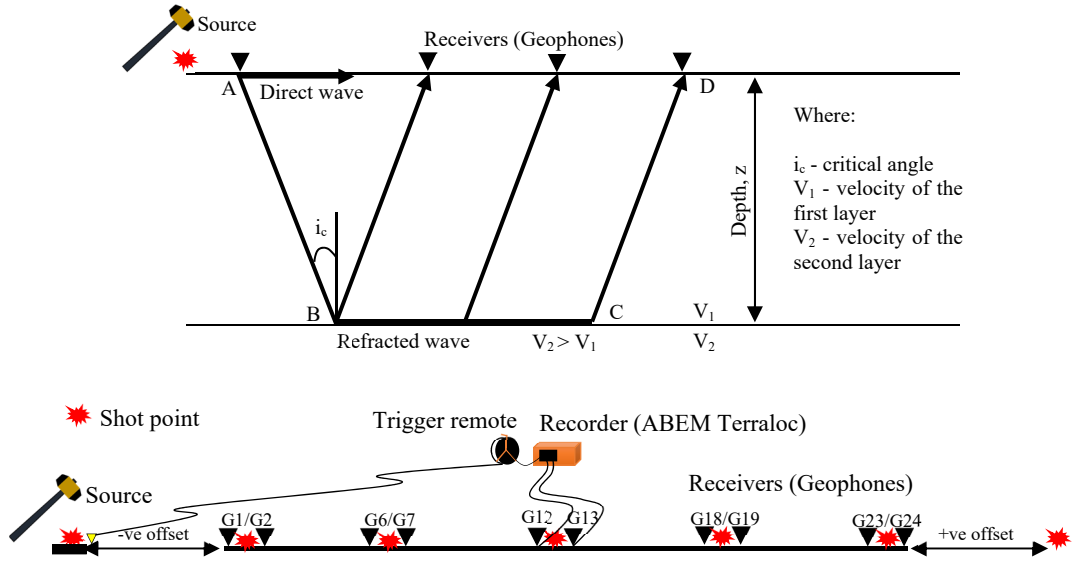

Fig. 4 Anatomy of SRT mechanism.

is used to estimate the depths to the failure and lateral extent of the landslide (Abidin et al., 2012; Yilmaz and Kamachi, 2018). This estimation is based on differences in the physical properties of the sliding materials and the underlying undisturbed sediments or bedrock, resulting in different seismic velocities (Abramson et al., 2002). The underlying principle behind the SRT method is the measurement of travel times of the seismic waves refracted at the interfaces between the subsurface layers of different velocities. The wave travels directly through the upper layer (direct arrivals), or it may travel down to and then laterally along with the high-velocity layers (refracted arrivals) before being propagated back to the surface (Fig. 4). A critical refracted wave travels along the interface between layers and is refracted back into the upper layer at the critical angle. The thickness and velocity of the material above and below an interface can be calculated by determining the arrival times of the direct and refracted waves from the seismic section (Saad et al., 2017).

Seven shot points were acquired to provide dense velocity distribution with five inline shot points, while the others as positive and negative offsets. Inline shot points are located at the middle of geophone (G); G1-G2, G6-G7, G12-G13, G18-G19, and G23-G24. FIRSTPIX v4.21 software was used to pick the first arrival time from the 24 traces for each shot point. The picked traces were subsequently subjected to travel time analysis, and corrections were applied to the initially picked values. Any inaccuracies identified in the initial stage were rectified using travel times obtained from both forward and reverse shooting for reciprocal time correction. Accurate picking is crucial to ensure the reliability of the generated velocity model. Hence, the final output comprises a depth profile of the refractor layers and a velocity generated by calculating the ray path tracing of arrival time for every shot point using SeisOpt@2D software. It operates using a nonlinear optimisation method known as adaptive simulated annealing, which involves forward modelling. Test velocity models were generated, through which travel time was determined. The calculated travel time was then compared with the observed data, and the errors between them were optimised, thus generating velocity models with minimum travel time errors. Figure 5 shows the overview of SRT data processing.

3. RESULTS

3.1. ERI

Figure 6a shows the result of line BR1, where the saturated zone was identified with a resistivity value of <100 Ωm. The highly weathered zone suspected with resistivity ranges of 100–1200 Ωm at depth of <60 m. The boulder and granite outcrop were identified at high resistivity range of 1200-3500 Ωm at distances of 80 m and 135–165 m, respectively. Figure 6b shows the BR2 profile with a survey length of 400 m and depth investigation up to 100 m. In these profiles, three distinct zones were classified. The 1st zone which is characterises as a highly weathered zone with the resistivity values ranging from 100–1200 Ωm, at depths of <30 m from the surface. The saturated zone and boulder were identified at resistivity values of <100 Ωm and 1200–3500 Ωm, respectively. The second zone, 2nd located at depths of >30 m, is marked by a weathered zone with a resistivity range of 3500–5000 Ωm, while third zone, 3rd representing bedrock, exhibits resistivity values of >5000 Ωm.

The subsurface characteristics of BR2 show high similarities in BR9 profiles as saturated zone and highly weathered were identified at resistivity of <100 Ωm and 1200–3500 Ωm, respectively. The highly weathered zone was located at depth of <30 m

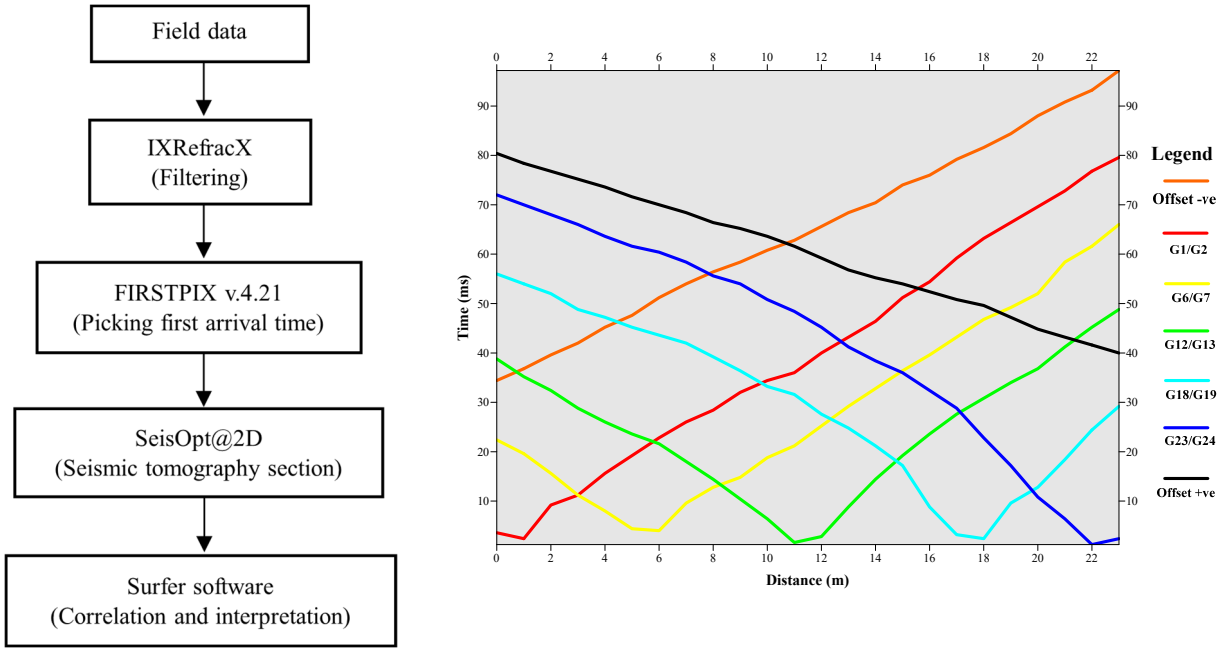

Fig. 5 Flow chart of SRT data processing with the example of travel time analysis.

from the surface. The weathered zone identifies at depth of <40 m with resistivity ranging from 3500–5000 Ωm. The bedrock was clearly observed with high resistivity values of >5000 Ωm. BR4 and BR6 show the saturated zone (<100 Ωm) dominated by a highly weathered zone with the resistivity of 100–1200 Ωm at a depth of <70 m. The boulder was indicated by the resistivity of 1200–3500 Ωm at a depth of <15 m, as shown in Figure 6d.

Figure 7 shows the inversion model of ERI for line BR3, BR5, BR7, and BR8. These four lines was located inside the landslide area. Generally, the result shows similarity in features as the previous lines where highly weathered zones were found at a depth of <70 m with resistivity values of 100–1200 Ωm. Figure 7a and Figure 7b for line BR3 and BR5 clearly shown the highly weathered zone as the saturated zone as identified at a resistivity of <100 Ωm. The boulder was identified at resistivity values ranges of 1200–3500 Ωm. Weathered zone with a resistivity of 3500–5000 Ωm was identified as shown in Figure 7a and Figure 7b. Figure 7c and Figure 7d show the result of lines BR7 and BR8 where the highly weathered zone was dominated with saturated zone at resistivity value of <100 Ωm. The result shows the granitic bedrock with resistivity values of >5000 Ωm at the depth of 20–40 m.

3.2. SRT

Figure 8 illustrates the SRT results of BS1–BS2 in the study area with a velocity, V_p ranges from 300–4200 m/s with a depth of penetration up to 20 m. The survey lines are oriented parallel to the slope for both BS1 and BS2. The survey for both profiles depicted three different velocity layers: 1st layer identified with velocity, V_p =300–600 m/s at depth <5 m; 2nd layer identified at 800-2400 m/s; and 3rd layer at velocity of V_p >2600 m/s. The 1st layer is interpreted as containing less loose material or soil at depths less than 5 m, while the 2nd layer corresponds to the weathered granite in the area. The 3rd layer is characterized as the bedrock for both profiles.

4. DISCUSSION

4.1. ERT AND SRT

From both profiles of ERI and SRT, several components could drive instability, such as the presence of saturated zones, boulders, and highly weathered/loose materials or less compacted soil (Noviyanto et al., 2020). The saturated zone represents high water saturation as dominated at depth of <10 m. The low resistivity region may indicate material composed of moist material of silt, representing a weak zone with a high water–bearing capacity (Ismail et al., 2019). The low velocity in that region with soft to medium stiffness could indicate the weak zone of the profile due to the presence of a high-water saturation zone. Previous site investigations by Mariappan et al. (2010), revealed three dominant types of soil layers identified as silt, sandy gravel, and granite. Finer materials like silt have higher water–bearing capacity compared to coarser materials like sand. Soil with high porosity and less clay content is less saturated with water, whereas material with high clay content could store water (good water–bearing) and increase mass, potentially inducing instability (Ismail et al., 2019). The existence of weathered granite layer with a velocity of

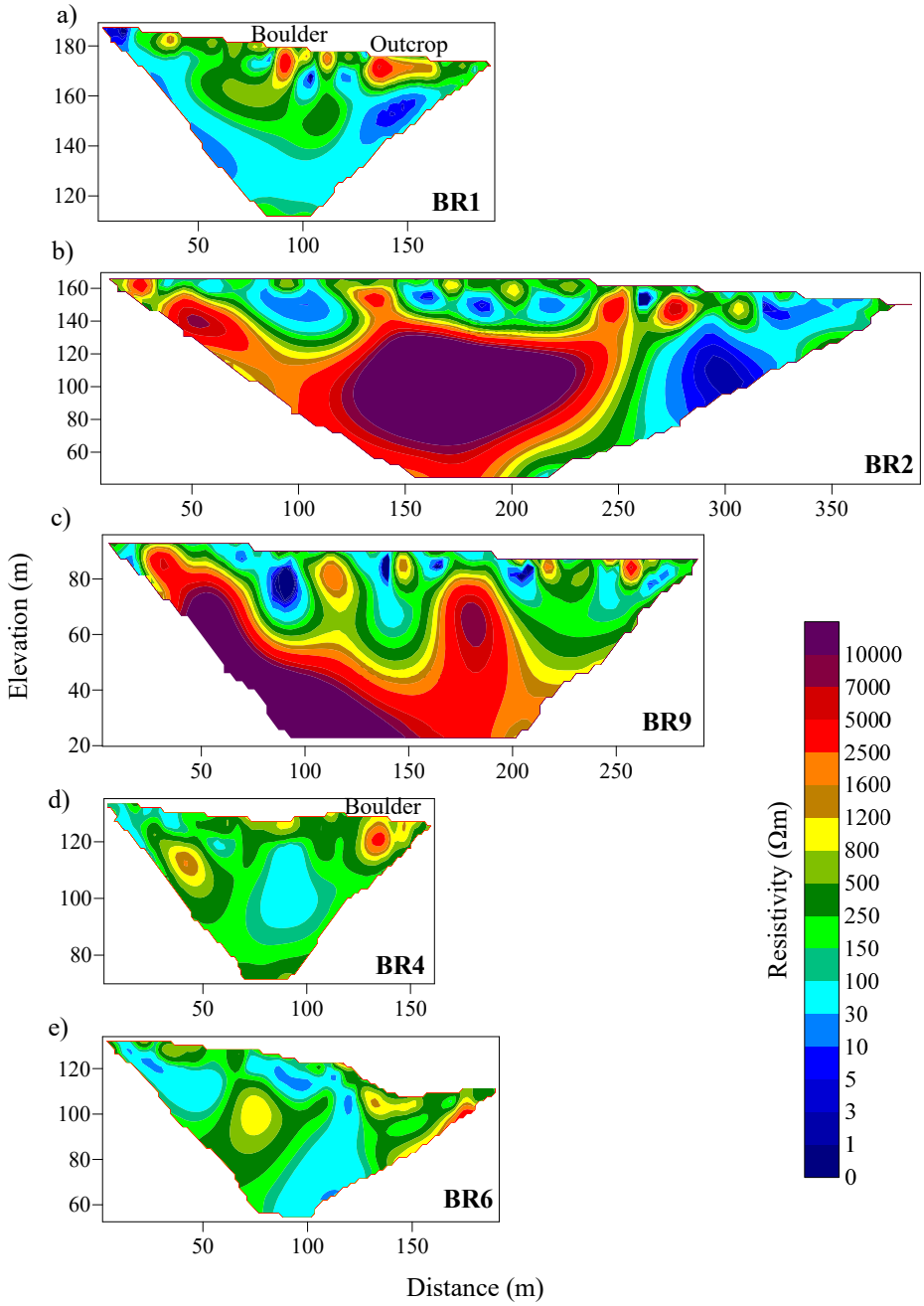

Fig. 6 Inversion models of ERI – parallel to the slope (*outside from landslide boundary*); a) BR1; b) BR2; c) BR9; d) BR4; e) BR6.

V_p =1200–2400 m/s and the presence of a high saturation region of <100 Ωm contribute additional factors to instability. For example, in profile BS2, the highly weathered material at a depth of <10 m represents colluvium with velocity values of V_p <1200 m/s, indicating less compacted or loose material in this area. Throughout the survey, two prominent zones, the high saturation zone and high resistivity materials, were identified. The high saturation zone from the surface indicates an unstable zone, which could trigger surface erosion (Lech et al., 2020). High resistivity (>5000 Ωm) with a low saturation zone, characterized by high velocity (V_p >2600 m/s), shows the bedrock of this area. High velocity and resistivity values indicate increasing soil stiffness as a medium to stiff layer (Lee–In et al., 2014).

4.2. CORRELATION OF PROFILES WITH BOREHOLE

The geophysical results are correlated with inlines boreholes to provide more reliable informations. Figure 9 shows the correlated result with inlines boreholes. The ERI and SRT survey lines of BR2 and BS1 were correlated with borehole BH8, as depicted in Figure 9a. The borehole was located at distances of 205 m and 120 m for ERI and SRT profiles, respectively.

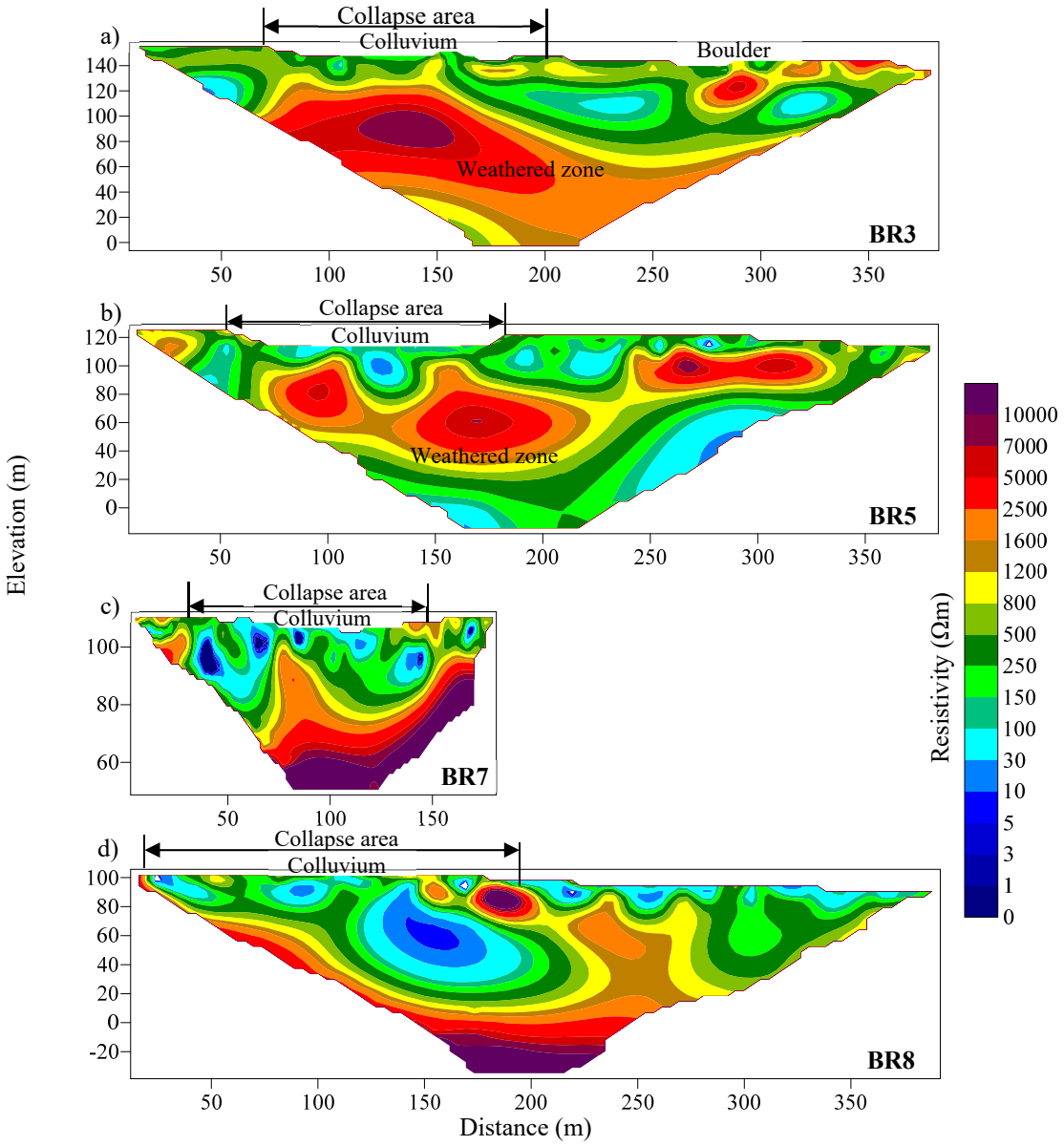

Fig. 7 Inversion models of ERI–parallel to the slope (*inside landslide area*); a) BR3; b) BR5; c) BR7; d) BR8.

In the ERI profiles, values exhibit variation with depth, whereas the SRT profile demonstrates proportional increases in velocity with depth, correlating with the varying N-values indicating the number of blows. At depths of <10 m, the resistivity shows the values ranges of 300–1200 Ωm while velocity shows ranges of V_p =300–1000 m/s. These depth profiles indicate that the subsurface is highly weathered due to low resistivity and velocity, suggesting these profiles contain less compacted or loose material. The N–value at this depth show values of <20 blows, which strongly indicate that the layer was highly weathered. The presence of a boulder is indicated at depths ranging from 16–18 m and 19– 23 m, as shown in borehole profiles. The bedrock was identified at a depth of 29 m in the borehole profile, indicated by increasing velocity values exceeding 2800. The presence of a saturation zone (<100 Ωm) at a depth of less than 30 m, along with a low distribution of N–values and the presence of a boulder, creates unstable and weak conditions for the slope. The increasing force introduced by the additional mass of the boulder contributes to slope failure by surpassing downward forces against the slope's shear strength. Simultaneously, the shear strength of soil decreases with an increase in water content (Omar et al., 2018).

The cohesion of materials, resulting from the bonding between the surfaces of particles, is affected by changes in moisture content. As the pore spaces are filled with water, the weight of soils increases, leading to instability (Ismail et al., 2019). The other profiles show high similarities trends of the subsurface materials. The low zone of N–values (1–15 blows)

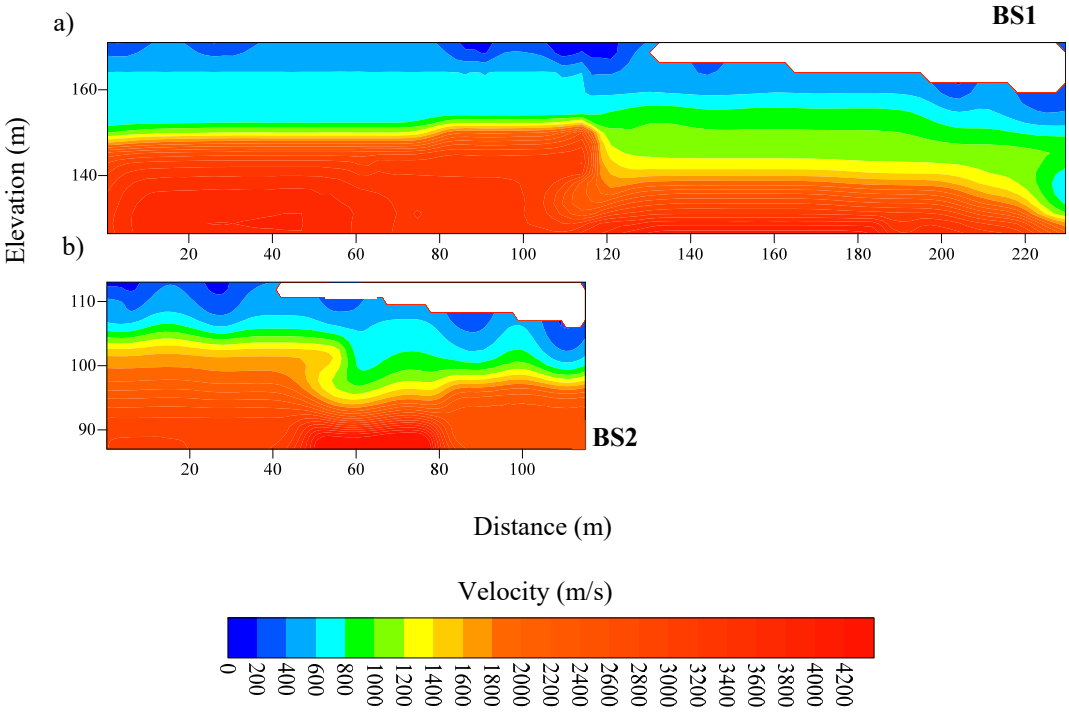

Fig. 8 SRT models; a) BS1; b) BS2.

Table 2 Summary of the boreholes.

Borehole	Resistivity (R)	Seismic (S)	Distance (m)	End of Depth (m)	Boulder Depth (m)	Rock Head (m)
BH8	BR2	BS1	(R) 205; (S) 120	32.3	10.0-18.0; 19.0-22.7	29.3
BH6	BR3	-	55	13.5	8.7-9.0	-
BH4	BR4	-	105	30.5	-	28.7
BH25	BR5	-	105	20.4	-	15.4
BH1	BR9	-	20	23.0	-	22.0

indicates highly weathered materials with resistivity <800 Ωm, considered as soft to medium-stiff materials. Lower N–values are strongly associated with loose materials, indicating a progressive weathering process (Tan Akip et al., 2018). An increasing number of N–values (15–30 blows) at resistivity values of 1200–3500 Ωm could indicate the presence of a weathered granite layer or a boulder. Bedrock was identified at N–values of 50 blows, with resistivity values >3500 Ωm at depths ranging from 25–30 m. Table 2 summarizes the borehole records for this study.

5. CONCLUSION

ERI and SRT were employed to delineate the weak zone of the failure plane and subsurface characteristics of the slope. The study area reveals a highly weathered zone identified at resistivity values of <1200 Ωm with a velocity layer of V_p <1200 m/s. The N–values show variations in the number of blows with depth, suggesting that the layer may not be competent due to the present heterogeneous material resulting from a highly weathered process. In this study, the saturated zone is identified at resistivity values of <100 Ωm. Most of the ERI survey lines exhibit low resistivity values at the top layer of the profiles, as discussed previously. Additional factors, such as the presence of a fracture zone and boulder, accelerate the mechanisms leading to the occurrence of landslides.

As mentioned earlier, the low resistivity zones (<100 Ωm) at the top surface of the layer are associated with rainfall activities and the area's climate conditions. The low resistivity region (<100 Ωm) as saturated zones may be correlated with the high permeability of water-bearing fractures (Ramirez and Daily, 2001; Cavinato et al., 2006). In BR1–BR9 (Fig. 10), water circulation may be relatively shallow at this location. The infiltration of surface water might indicate the presence of saturated zones at a very shallow depth, about <3 m. The continuous infiltration of surface water, particularly during heavy rain, as it

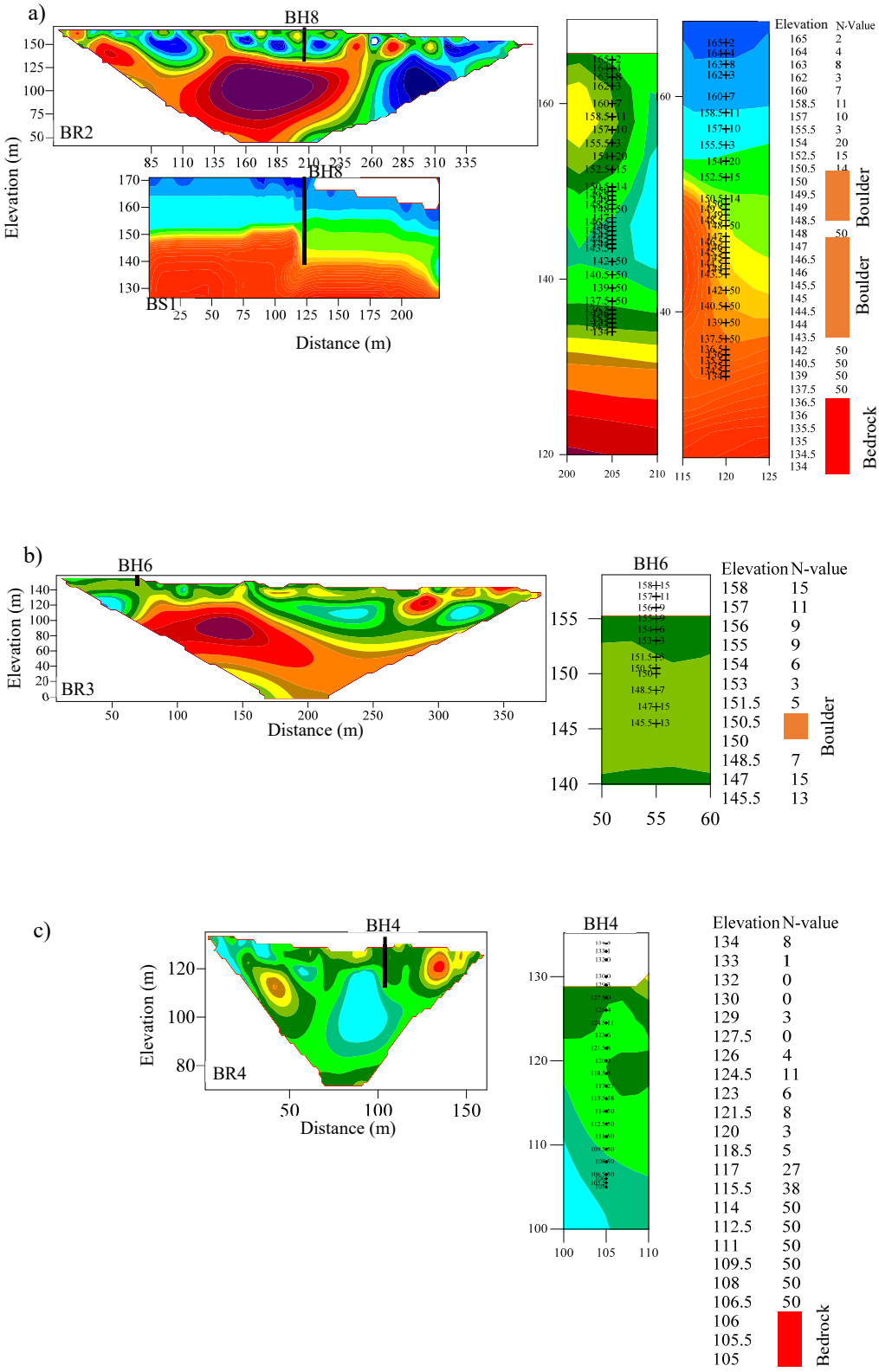
a)
BH8
BR2
BH8
BS1
Elevation (m)
Distance (m)
Elevation N-Value
Boulder
Boulder
Bedrock
b)
BH6
BR3
Elevation (m)
Distance (m)
BH6
Elevation N-value
Boulder
c)
BH4
BR4
Elevation (m)
Distance (m)
BH4
Elevation N-value
Bedrock

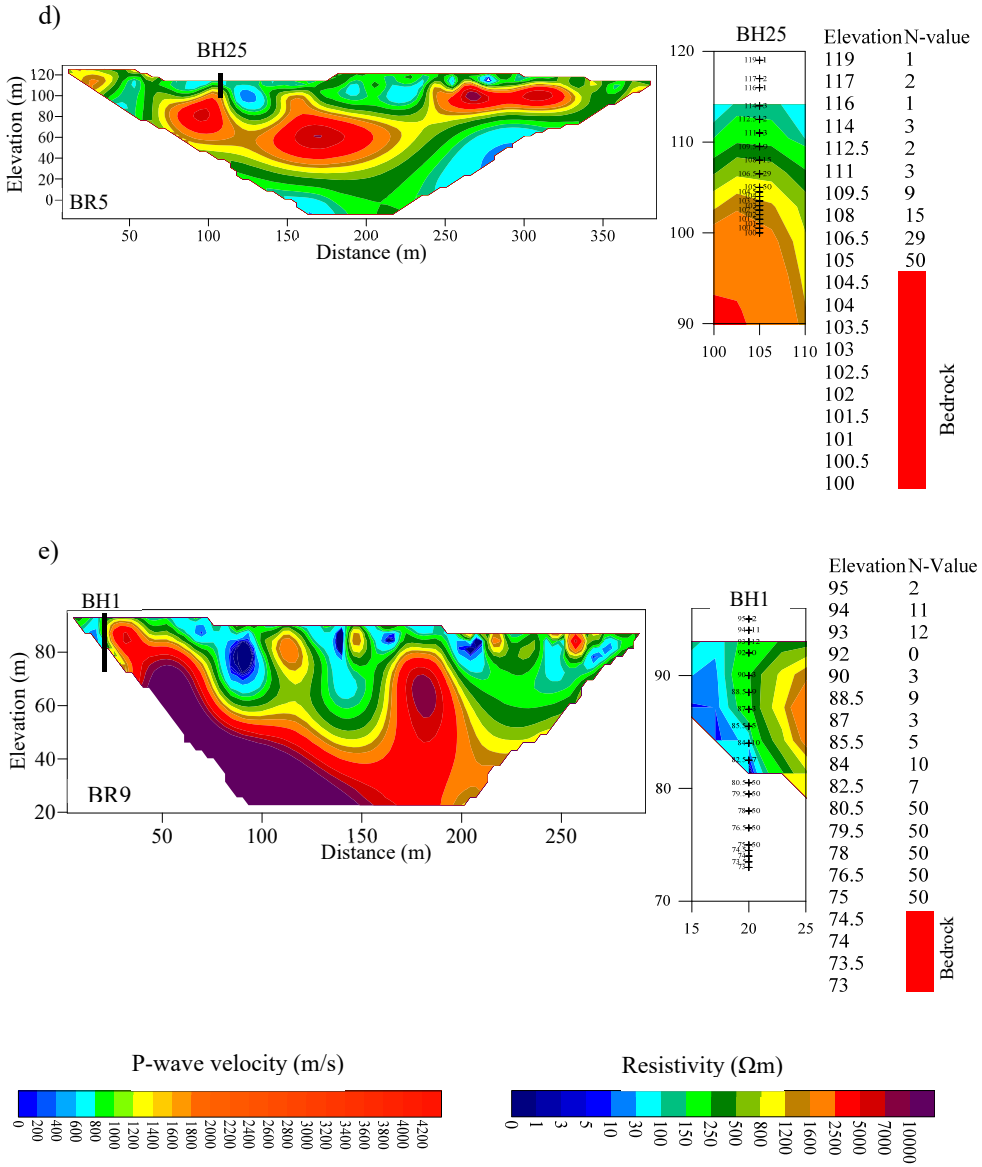

Fig. 9 Integrated result of geophysical models and borehole record; a) BR2&BS1–BH8; b) BR3–BH6; c) BR4–BH4; d) BR5–BH25; e) BR9–BH1.

seeps through to the fracture area and accumulates, may trigger slope instability, as the permeability and porosity of the soil are high. The disturbance of soil properties with variations in porosity and permeability increases the soil's effective stress, potentially triggering mass movement for slope instability (Zakaria et al., 2020). The unstable condition with loose materials and increased water accumulation contributes to the occurrence of slope failure (Beyabanaki et al., 2016).

ACKNOWLEDGEMENT

The authors wish to thank, all staffs, and postgraduate students from geophysics section Universiti Sains Malaysia (USM) for their assistance during the geophysical data acquisition. The authors thank to Ministry of Higher Education Malaysia for Fundamental Research Grant Scheme with Project Code: FRGS/1/2022/STG08/USM/03/1 entitle Performance-Based Multimodal Geophysical Design for Soil Dynamic Properties to Improve Visualisations of Subsurface Conditions.

REFERENCES

Abidin, M.H.Z., Saad, R., Ahmad, F., Wijeyesekera, D.C. and Tajul Baharuddin, M.F.: 2012, Seismic refraction tomography investigation on near surface landslides at the Kundasang area in Sabah, Malaysia. Procedia Eng., 50, 516–531.
DOI: 10.1016/j.proeng.2012.10.057

a)

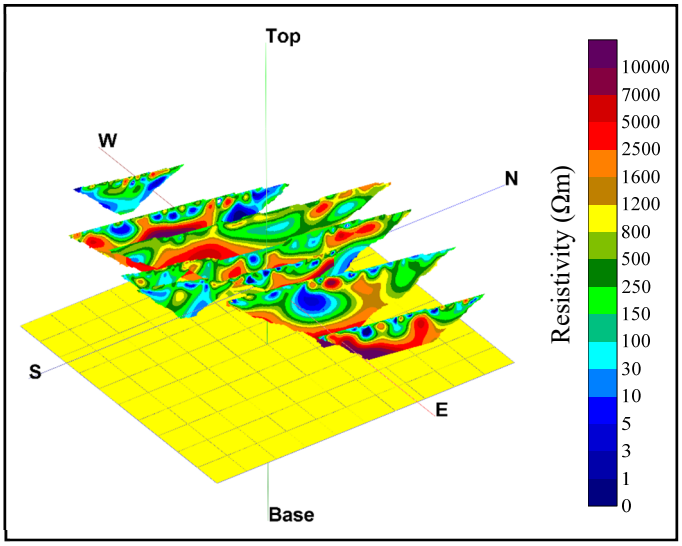

b)

Soil description	Layer 1 (1st)	Residual soil; Unconsolidated materials of soil/loose material/Highly weathered zone
	Layer 2 (2nd)	Weathered zone which may indicate the loose material or weathered granite.
	Layer 3 (3rd)	Weathered bedrock
	Thickness (m)	1st: <20 2nd: 5–20 3rd: 20–30
Geophysical values	Resistivity, ρ (Ωm)	1st: <1200 2nd: 1200–3500 3rd: >3500
	Velocity, V_p (m/s)	1st: <1200 2nd: 1200–2400 3rd: >2600

Fig. 10 a) 3–D orientation of ERI for S–N direction; b) Summary of the result for ERT and SRT profiles.

Abramson, L.W., Lee, T.S., Sharma, S. and Boyce, G.M.: 2002, Slope stability and stabilization methods, New York, NY, John Wiley and Sons, 736 pp.

Ali, F.H. and Huat, B.B.K.: 2006, Shallow foundation. In: Huat, B.B.K., Ali, F.H., Omar, H. and Singh, H. (Eds.): Foundation Engineering: Design and Construction in Tropical Soils. London, A.A. Balkema, 71–90.

Ali, F.H. and Rahardho, H.: 2004, Unsaturated residual soil. In: Huat, B.B.K., Sew, G.S. and Ali, F.H. (Eds.), Tropical Residual Soils Engineering, London, A.A. Balkema, 99–125.

Beyabanaki, S.A.R., Bagtzoglou, A.C. and Anagnostou, E.N.: 2016, Effects of groundwater table position, soil strength properties and rainfall on instability of earthquake-triggered landslides. Environ. Earth Sci., 75, 4, 1–13. DOI: 10.1007/s12665-016-5277-2

Beyene, A., Tesema, N., Fufa, F. and Tsige, D.: 2023, Geophysical and numerical stability analysis of landslide incident. Heliyon, 9, 3, 10–14. DOI: 10.1016/j.heliyon.2023.e13852

Cavinato, G.P., Di Luzio, E., Moscatelli, M., Vallone, R., Averardi, M., Valente, A. and Papale, S.: 2006, The new Col di Tenda tunnel between Italy and France: integrated geological investigations and geophysical prospections for preliminary studies on the Italian side. Eng. Geol., 88,1-2, 90–109. DOI: 10.1016/j.enggeo.2006.09.001

Christopher, W.A.P.P., De Silva, N., Attanayake, A.M.A.N.B. and Jayasingha, P.: 2023, Characterization of landslides: a vertical electrical sounding approach. Geosci. Lett., 10, 18. DOI: 10.1186/s40562-023-00274-x

Chigira, M., Mohamad, Z., Sian, L.C. and Komoo, I.: 2011, Landslides in weathered granitic rocks in Japan and Malaysia. Bull. Geol. Soc. Malaysia, 57, 1–6. DOI: 10.7186/bgsm57201101

Huat, L.T., Ali, F. and Ibrahim, A.S.: 2012, An investigation on one of the rainfall–induced landslides in Malaysia. Electron. J. Geotech. Eng., 17, 435–449.

Hungr, O., Leroueil, S. and Picarelli, L.: 2014, The Varnes classification of landslide types, an update. Landslides, 11, 167–194. DOI: 10.1007/s10346-013-0436-y

Innocenti, A., Rosi, A., Tofani, V., Pazzi, V., Gargini, E., Masi, E.B., Segoni, S., Bertolo, D., Paganone, M. and Casagli, N.: 2023, Geophysical surveys for geotechnical model reconstruction and slope stability modelling. Remote Sens., 15, 8, 2159. DOI: 10.3390/rs15082159

Ismail, N.E.H., Taib, S.H. and Abas, F.A.M.: 2019, Slope monitoring: an application of time-lapse electrical resistivity imaging method in Bukit Antarabangsa, Kuala Lumpur. Environ. Earth Sci., 78, 14, 1–15. DOI: 10.1007/s12665-018-8019-9

Kayode, J.S., Arifin, M.H. and Nawawi, M.O.H.D.: 2019, Characterization of a proposed quarry site using multi–electrode electrical resistivity tomography. Sains Malays., 48, 5, 945–963. DOI: 10.17576/jsm-2019-4805-03

Kazmi, D., Qasim, S., Harahap, I.S.H. and Vu, T.H.: 2017, Analytical study of the causes of the major landslide of Bukit Antarabangsa in 2008 using fault tree analysis. Innov. Infrastruct. Solut., 2, 55, 1–11. DOI: 10.1007/s41062-017-0105-4

Kearey, P., Brooks, M. and Hill, I.: 2013, An Introduction to Geophysical Exploration. Oxfordshire, Oxford, Blackwell Science, 288 pp.

Lech, M., Skutnik, Z., Bajda, M. and Markowska–Lech, K.: 2020, Applications of electrical resistivity surveys in solving selected geotechnical and environmental problems. Appl. Sci., 10, 7, 2263. DOI: 10.3390/app10072263

Lee–In, M., Kim, J.S., Yoon, H.K. and Lee, J.S.: 2014, Evaluation of compressive strength and stiffness of grouted soils by using elastic waves. Sci. World J., 2, 215804. DOI: 10.1155/2014/215804

Loke, M.H.: 2011, Electrical resistivity surveys and data interpretation. In: Gupta, H. (Ed.): Solid Earth Geophysics Encyclopedia, Electrical and Electromagnetic. Springer–Verlag, Heidelberg, Berlin, 276–283.

Malet, J.P., Van Asch, T.W., Van Beek, R. and Maquaire, O.: 2005. Forecasting the behaviour of complex landslides with a spatially distributed hydrological model. Nat. Hazards and Earth Syst. Sci., 5, 1, 71–85. DOI: 10.5194/nhess-5-71-2005

Marcato, G., Mantovani, M., Pasuto, A., Zabuski, L. and Borgatti, L.: 2012, Monitoring, numerical modelling and hazard mitigation of the Moscardo landslide (Eastern Italian Alps). Eng. Geol., 128, 95–107. DOI: 10.1016/j.enggeo.2011.09.014

Mariappan, S., Ashaari, M., Low, T.H., Nik, R.N.H., Chong, S. and Subramaniam, S.: 2010, Remedial measures adopted for slope failure at Bukit Antarabangsa, Malaysia. Proc. International Conference on Slope 2010, Chiang Mai, Thailand, 27–30 July 2010, 11–16.

Merghadi, A., Yunus, A.P., Dou, J., Whiteley, J., ThaiPham, B., Bui, D.T., Avtar, R. and Abderrahmane, B.: 2020, Machine learning methods for landslide susceptibility studies: a comparative overview of algorithm performance. Earth–Sci. Rev., 207, 103225. DOI: 10.1016/j.earscirev.2020.103225

Noviyanto, A., Sartohadi, J. and Purwanto, B.H.: 2020, The distribution of soil morphological characteristics for landslide–impacted Sumbing Volcano, Central Java – Indonesia. Geoenvironmental Disasters, 7, 1, 1–19. DOI: 10.1186/s40677-020-00158-8

Omar, R.C., Baharuddin, I.N.Z., Taha, H., Roslan, R., Khalid, N.H.N. and Muzad, M.F.: 2018, Slope stability analysis of granitic residual soil using slope/w, resistivity and seismic. Int. J. Eng. Technol., 7, 4, 172–176. DOI: 10.14419/ijet.v7i4.28.22355

Pazzi, V., Morelli, S. and Fanti, R.: 2019, A review of the advantages and limitations of geophysical investigations in landslide studies. Int. J. Geophys., 4, 1–28. DOI: 10.1155/2019/2983087

Rahman, H.A. and Mapjabil, J.: 2017, Landslides disaster in Malaysia: an overview. Health Environ. J., 8, 1, 58–71.

Ramirez, A. and Daily, W.: 2001, Electrical imaging at the large block test—Yucca Mountain, 1173 Nevada. J. Appl. Geophys., 46, 2, 85–100. DOI: 10.1016/S0926-9851(00)00042-2

Rosso, R., Rulli, M.C. and Vannucchi, G.: 2006, A physically based model for the hydrologic control on shallow landsliding. Water Resour. Res., 42, 6, 1–16. DOI: 10.1029/2005WR004369

Saad, R., Muztaza, M.N., Zakaria, M.T. and Saidin, M.M.: 2017, Application of 2D resistivity imaging and seismic refraction tomography to identify Sungai Batu sediment depositional origin. J. Geol. Geophys., 5, 7, 1–5. DOI: 10.4172/2381-8719.1000268

Tan Akip, S.M., Tonnizam, M.E., Saad, R., Dan, M.M., Nordiana, M. M., Hazreek, Z. A.M. and Madun, A.: 2018, Correlation of resistivity value with geotechnical n–value of sedimentary area in Nusajaya, Johor, Malaysia. J. Phys. Conf. Ser., 995, 1, 1–14. DOI: 10.1088/1742-6596/995/1/012079

Whiteley, J.S., Chambers, J.E., Uhlemann, S., Wilkinson, P.B. and Kendall, J.M.: 2019, Geophysical monitoring of moisture-induced landslides: A review. Rev. Geophys., 57, 1, 106–145. DOI: 10.1029/2018RG000603

Yilmaz, S. and Kamaci, Z.: 2018, Resistivity and seismic refraction studies on Kısıklı landslide (Antalya, Turkey). International Journal of Computational and Experimental Science and Engineering, IJCESEN, 4, 3, 9–14. DOI: 10.22399/ijcesen.348792

Yordkayhun, S.: 2021, Geophysical characterization of a sinkhole region: A study toward understanding geohazards in the karst geosites. Sains Malays., 50, 7, 1871–1884. DOI: 10.17576/jsm-2021-5007-04

Zaid, H.A.H., Arifin, M.H., Kayode, J.S. and Iswadi, M.B.: 2023, Application of 2–d electrical resistivity imaging, and induced polarization methods for delineating gold mineralization at Felda Chiku 3, Kelantan, Malaysia. Sains Malays., 52, 1, 305–320. DOI: 10.17576/jsm-2023-5201-25

Zakaria, M.T., Mohd Muztaza, N., Zabidi, H., Salleh, A.N., Mahmud, N., Samsudin, N., Rosli, F.N., Olugbenga, A.T. and Jia, T.Y.: 2021, 2–D cross–plot model analysis using integrated geophysical methods for landslides assessment. Appl. Sci., 11, 2, 747. DOI: 10.3390/app11020747

Zakaria, M.T., Muztaza, M.N., Zabidi, H., Ahmad, F., Adeeko, T.O., Ismail N. and Samsudin, N.: 2020, Slope instability evaluation using geophysical methods of Gua Musang–Cameron Highland highway. Lowl. Technol. Int., 22, 1, 172–177.

Zakaria, M.T., Muztaza, N.M., Zabidi, H., Salleh, A.N., Mahmud, N. and Rosli, F.N.: 2022, Integrated analysis of geophysical approaches for slope failure characterisation. Environ. Earth Sci., 81, 10, 299. DOI: 10.1007/s12665-022-10410-z